INORGANIC CHEMISTRY
FRONTIERS

RESEARCH ARTICLE

View Article Online
View Journal

Cite this: DOI: 10.1039/d4qi03209h

Dual non-noble-metal-immobilized covalent organic frameworks for visible-light-driven photocatalytic hydrogen evolution†

Mengjiao Shao, Aodi Wang, Jiani Peng, Xueling Song and Lei Wang *

Covalent organic frameworks (COFs) have emerged as highly versatile platforms for the spatially controlled immobilization of metals in heterogeneous photocatalytic hydrogen evolution reactions (HERs). Herein, we have integrated both a Cu(I) diimine-based photosensitizer unit and a Co(II) bipyridine-based catalyst unit into a two-dimensional COF, TpBpy, which serves as a macro-ligand scaffold. The resulting hybrid material, TpBpy–Cu/Co, achieves an optimized photocatalytic H_2 evolution rate of 12.16 mmol g^{-1} h^{-1}, representing a 25-fold enhancement relative to the pristine TpBpy framework. To elucidate the origin of this enhancement, ultrafast transient optical spectroscopy, electrochemical measurements, and photoluminescence studies were employed. These studies reveal that the incorporation of the Cu(I) diimine unit enhances the photosensitizing capability of the framework, while the excited-state lifetime of the photosensitizer is prolonged due to the confinement effects within COF structure. Furthermore, comparative invetigations demonstrate that the TpBpy–Cu/Co outperformes the system consisting of separate TpBpy–Cu and Co(bpy)Cl_2, highlighting the critical role of metal coordination in facilitating intra-framework charge transfer from photosensitizers to catalysts. This study provides strategic insights into the design of COF–metal coordination systems, emphasizing the importance of integrating multifunctional units to tailor and enhance photocatalytic performance.

Received 13th December 2024,
Accepted 14th May 2025

DOI: 10.1039/d4qi03209h

rsc.li/frontiers-inorganic

Introduction

Solar energy conversion is a critical and effective strategy for addressing the dual challenges of the global energy crisis and environmental problems.[1,2] Substantial progress has been made over the past several decades in the synthesis and development of novel materials for the generation of sustainable and alternative energy sources, particularly hydrogen.[3–5] The unique properties of covalent organic frameworks (COFs), such as high surface area, effective visible light absorption, and tunable structural and electronic characteristics, make them as advanced alternatives to conventional photocatalytic materials.[6–8] Nevertheless, the high intrinsic impedance of organic materials result in low charge transfer efficiency within photocatalytic systems. This limitation underscores the necessity for further research aimed at optimizing the charge dynamics in COF-based photocatalysts to enhance their overall efficiency and performance in solar energy conversion applications.[9–12]

Specifically, incorporating metal ions into the backbones of COFs has received much attention to enhance photocatalytic performance by mitigating carrier-transfer impedance and broadening light absorbance.[13,14] In this regard, multidentate ligands have been designed as foundational building blocks for two-dimensional COFs. Bipyridine-containing COFs have gained significant attention due to the inherent redox stability of bipyridine and the presence of coordination sites that promote metal ion integration as well as the wide availability of bipyridine-type ligands.[15–17] So far, researchers have successfully incorporated a range of metal ions, including Co(II),[18] Ni(II),[19] Cu(II), Ru(II),[20,21] and Ir(II),[21] into bipyridine-based COFs, especially TpBPy. The resulting TpBPy–M frameworks generally exhibit effective charge interactions between the TpBPy ligand and the metal centers, leading to remarkable promotion in photocatalytic efficiency.[19] However, few of them applied insights from homogeneous metal complexes to develop TpBPy–M COFs.

In recent years, copper complexes have garnered significant attention in photocatalysis, primarily due to the abundant availability of copper (approximately 60 ppm). In par-

School of Materials and Chemistry, University of Shanghai for Science and Technology, Shanghai 200093, China. E-mail: leiwang@usst.edu.cn

† Electronic supplementary information (ESI) available. See DOI: https://doi.org/10.1039/d4qi03209h

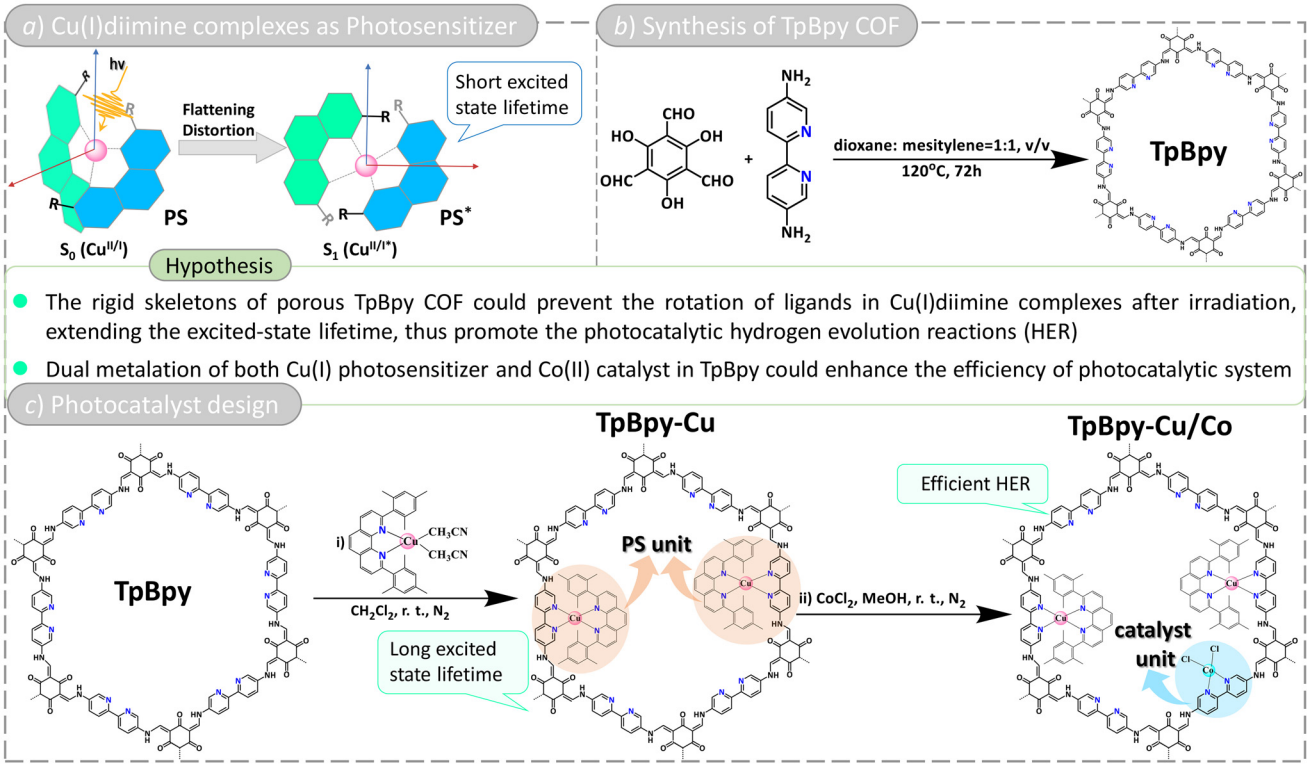

Fig. 1 (a) Cu(I) bis-phenanthroline complexes undergo ligand flattening when photoexcited. In the ground state (S_0), the ligands are nearly perpendicular to each other, while in the lowest singlet MLCT excited state (S_1), the molecule is flattened. Color indicators: Cu = pink, and phenanthroline ligands = blue and green. (b) Typical procedure for the synthesis of TpBpy COF. (c) Photocatalyst design based on fundamental understanding of metal complexes and synthesis *via* post-modification strategy in the TpBpy backbone. Color indicators: Cu(I) photosensitizer (PS) unit = orange, and Co(II) HER catalyst unit = blue.

ticular, Cu(I) diimine complexes have become increasingly vital as both electron donors and photosensitizers, attributed to their favorable metal-to-ligand electron transfer properties.[22–24] However, Cu(I) diimide complexes have unstable tetrahedral like configuration, which is easily converted into a quasi-square planar configuration after being excited by light. In this state, it becomes easy for the coordination solvent molecules to coordinate with the complex to form an "exciplex", which shortens the photosensitizer's excited state lifetime (Fig. 1a).[25] For the above reasons, bulky substituents were introduced at the 2,9 positions of 1,10-phenanthroline ligands, aiming to limit spatial torsion and molecular structure distortion.[26]

Consequently, we propose that the porous structure of COFs can confine the ligands in a limited space within COFs and thus optimize the photosensitizing properties of Cu(I) diimine complexes. At the same time, $Co(bpy)Cl_2$ has been widely studied for its role in catalytic hydrogen production, demonstrating considerable efficacy.[27,28] However, the practical application of these non-noble-metal complexes is often hindered by challenges associated with recycling efficiency and the difficulty of product separation. To address these limitations, the heterogenization of these homogeneous molecular complexes is regarded as a promising approach.

Building on the above insights, this work utilizes TpBpy COF as a heterogeneous platform to covalently incorporate Cu(I) diimine as a photosensitizer unit and Co(II) as a catalyst unit (Fig. 1b and c). We anticipated that the resulting metallated framework, TpBpy–Cu/Co, would exhibit superior photocatalytic hydrogen evolution reaction (HER) efficiency compared to the unmodified TpBpy COF and its homogeneous counterparts due to: (1) the pore confinement effect of the rigid skeletons, which improves the performance of the Cu(I) photosensitizer and (2) metal coordination improves charge separation and transfer efficiency. Interestingly, TpBpy–Cu/Co exhibited remarkable long-term stability, maintaining photocatalytic activity for up to 24 h. This study demonstrates a novel approach that applies insights from homogeneous catalysis to modify COFs with dual non-noble-metals, thereby significantly improving the photocatalytic performance of heterogeneous systems.

Results and discussion

Synthesis and characterization

The synthesis of the 2D COF containing 2,2′-bipyridine was achieved through a previously established solvothermal method. This process utilized 2,2′-bipyridine-5,5′-diamine

(Bpy-NH_2) and 1,3,5-triformylphloroglucinol (Tp) as building blocks. The reaction was conducted in a mixed solvent of dioxane and mesitylene (1 : 1, v/v) at a temperature of 120 °C for three days, employing acetic acid (6 M) as the catalyst (Fig. 1b).[29] The powder X-ray diffraction (PXRD) analysis of the synthesized TpBpy revealed distinct characteristic peaks at 3.8° and 26.8°, representing AA stacking (Fig. 2a). Subsequently, molecular units (a copper photosensitizer and a cobalt catalyst) were incorporated into the TpBpy COFs *via* a post-modification treatment. The synthesized TpBpy–Cu/Co exhibited a loss of crystallinity in contrast to individual TpBpy, a common phenomenon in COFs with post-metal coordination (Fig. S1†).[30] This loss is attributed to the disruption of π–π stacking interactions that stabilize the eclipsed packing of the layers. To restore the crystallinity of TpBpy–Cu/Co, we immersed the samples in dimethylsulfoxide (DMSO) for 48 h at room temperature according to a method reported previously.[30] As shown in Fig. 2b, the PXRD patterns of the recovered TpBpy–Cu/Co closely resemble those of the original TpBpy, confirming the restoration of crystallinity. However, a reduction in the intensity of the predominant diffraction peak at 26.8°, corresponding to the (001) facet, was observed. This decrease is likely due to the incorporation of larger molecular units into the COF framework, which contributes to partial disordering. Furthermore, inductively coupled plasma (ICP) spectroscopy was employed to accurately determine the metal contents, revealing that the coordinated Cu(I) and Co contents in the TpBpy–Cu/Co COF were 3.45% and 1.77%, respectively (Table S1†).

The success of the reaction was confirmed by solid-state nuclear magnetic resonance (NMR) spectroscopy and Fourier-transform infrared spectroscopy (FT-IR). Fig. S2† displays the NMR peaks from 100 to 200 parts per million for TpBpy–Cu, with chemical shifts and peak shapes characteristic of those expected for C=C double bonds.[21,31–33] As shown in Fig. 2c, the Fourier transform infrared (FT-IR) spectra of all three COFs exhibit a C–N stretching band at 1270 cm^{-1}, a C=C stretching band at 1451 cm^{-1}, and a stretching peak for the formyl

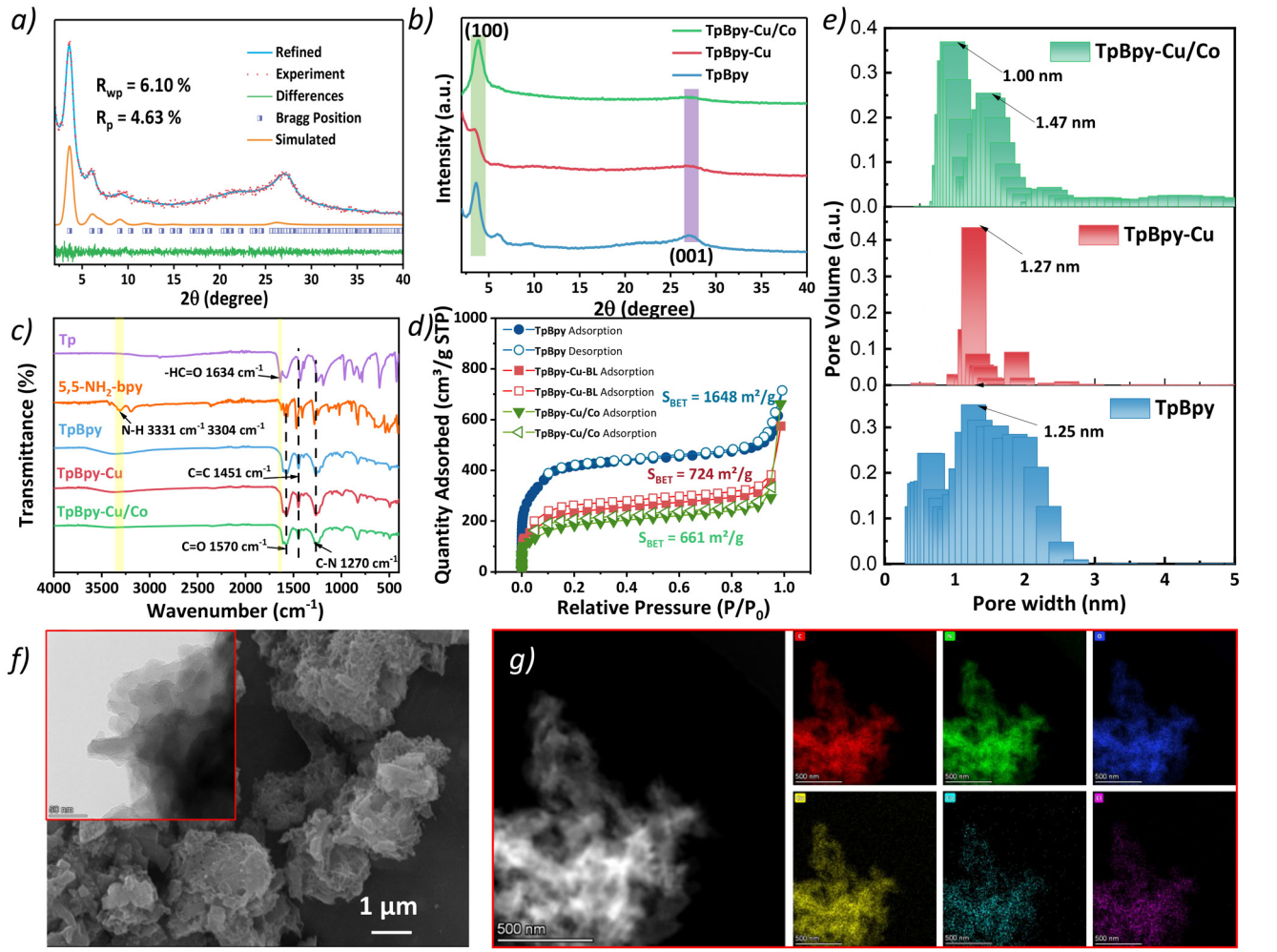

Fig. 2 (a) Experimental/simulated XRD pattern of the TpBpy COF. (b) Experimental PXRD patterns, (c) FT-IR spectra, (d) N_2 sorption isotherms, and (e) Pore size distribution of TpBpy, TpBpy–Cu, and TpBpy–Cu/Co. (f) SEM image (inset: TEM image) of TpBpy–Cu/Co. (g) EDS mapping images for TpBpy–Cu/Co.

groups (C═O) at 1570 cm^{-1}. The absence of the –CHO group at 1634 cm^{-1} and the $–NH_2$ group at 3331 cm^{-1} in the FT-IR spectra of TpBpy–Cu/Co provides evidence for the successful completion of the Schiff-base reaction. These findings also indicate the β-ketoenamine backbone remains unchanged during the post-modification process.

Nitrogen adsorption–desorption isotherms recorded at 77 K for TpBpy, TpBpy–Cu, and TpBpy–Cu/Co displayed a characteristic type-I profile, which is indicative of their microporous structure. The Brunauer–Emmett–Teller (BET) surface areas were found to be 1648 $m^2\ g^{-1}$ for TpBpy, 724 $m^2\ g^{-1}$ for TpBpy–Cu, and 661 $m^2\ g^{-1}$ for TpBpy–Cu/Co (Fig. 2d). Additionally, the pore size distributions for TpBpy and TpBpy–Cu were approximately 1.25 nm, while TpBpy–Cu/Co exhibited pore sizes of 1.00 nm and 1.47 nm. The decline in the BET surface area and the alteration in pore size distribution (Fig. 2e) are mainly attributed to the incorporation of metal ions within the pristine COF structure.

The morphology of the materials was examined using scanning electron microscopy (SEM) and transmission electron microscopy (TEM). As shown in Fig. 2f and Fig. S3, S4,† all materials retained the characteristic stacked-sphere morphology typical of 2D-COFs, indicating that the post-modification did not alter their structure. To further assess the distribution of metal elements, energy dispersive spectroscopy (EDS) analysis was conducted. Fig. 2g and Fig. S5, S6† show the uniform dispersion of Cu and/or Co across the COF surfaces, suggesting a well-distributed arrangement of the photosensitizer and catalyst units. This uniform dispersion facilitates close contact between Cu(I) and Co(II), which is critical for high catalytic efficiency.

X-ray photoelectron spectroscopy (XPS) provides a detailed assessment of the surface chemical composition of metal-modified TpBpy. The full XPS spectra confirm the presence of carbon, nitrogen, oxygen, and metal elements in TpBpy–Cu and TpBpy–Cu/Co, indicating the successful incorporation of photosensitizer and catalyst units (Fig. S7†). Additionally, elemental signals for counter ions, including phosphorus, fluorine, and chlorine, were also detected. The high-resolution N 1s XPS spectrum of TpBpy reveals two peaks at 398.2 eV and 400.1 eV, corresponding to pyridyl nitrogen atoms and secondary amines, respectively (Fig. 3a). However, significant changes are observed in the N 1s profiles of TpBpy–Cu and TpBpy–Cu/Co, the relative intensity of pyridyl nitrogen atoms was reduced compared to secondary amines for TpBpy–Cu and TpBpy–Cu/Co, indicating the formation of coordination bonds between nitrogen and the metal ions (Fig. 3b and c). Meanwhile, the high-resolution O 1s XPS spectra of TpBpy and TpBpy–Cu/Co were also compared, as shown in Fig. S8.† Characteristic peaks were observed for the keto oxygen bond at 531 eV and the enol oxygen at 533 eV with no obvious changes between the two samples, demonstrating that neither Cu–O nor Co–O coordination occurred, which further confirms the *N*,*N*-coordination environments of Cu and Co.[18,30] Furthermore, two distinct peaks at 402.6 eV and 403.6 eV were assigned to the

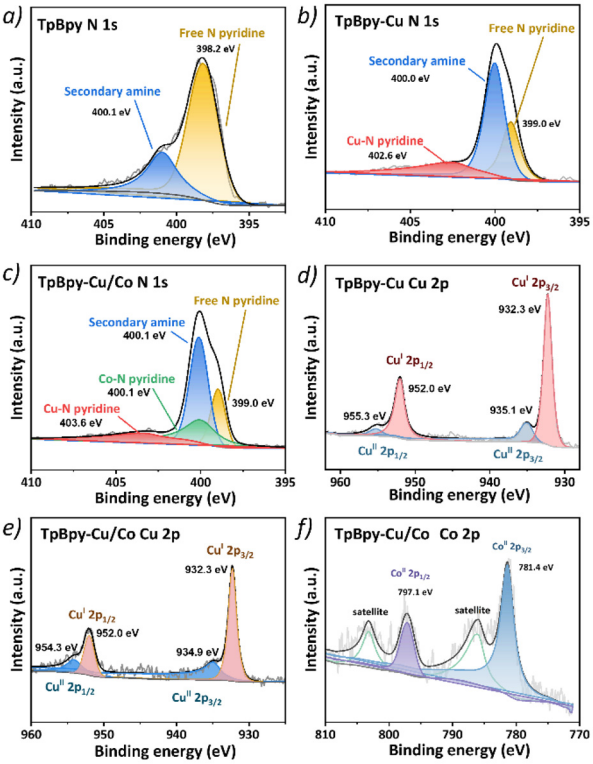

Fig. 3 (a-c) N 1s XPS spectrum of (a) TpBpy, (b) TpBpy–Cu and (c) TpBpy–Cu/Co. (d–e) Cu 2p XPS spectrum of (d) TpBpy–Cu and (e) TpBpy–Cu/Co. (f) Co 2p XPS spectrum of TpBpy–Cu/Co.

Cu–N binding energies in TpBpy–Cu and TpBpy–Cu/Co, respectively.[34] The XPS analysis also reveals the binding energies for Cu(I) $2p_{1/2}$ and Cu(I) $2p_{3/2}$ at 952.0 eV and 932.3 eV, respectively (Fig. 3d and e), confirming the presence of Cu(I) in TpBpy–Cu and TpBpy–Cu/Co.[30]

Additionally, small peaks at 954.3 eV and 934.9 eV, corresponding to Cu(II) $2p_{1/2}$ and Cu(II) $2p_{3/2}$, indicate that a minor portion of Cu(I) has been oxidized to Cu(II). The Co(II) 2p XPS spectrum of TpBpy–Cu/Co displays characteristic peaks at 781.4 eV ($2p_{3/2}$) and 797.1 eV ($2p_{1/2}$), confirming the presence of Co(II) (Fig. 3f).[18]

To analyze the energy band structures of TpBpy, TpBpy–Cu and TpBpy–Cu/Co, UV-Vis absorption spectroscopy and ultraviolet photoelectron spectroscopy (UPS) were performed. As shown in Fig. 4a, the UV-Vis absorption spectra indicate that all materials exhibit visible-light absorption. Based on these measurements, the optical band gaps were determined to be 2.23 eV for TpBpy, 2.16 eV for TpBpy–Cu, and 2.14 eV for TpBpy–Cu/Co, showing a slight decrease in the band gap upon metal incorporation (Fig. 4b). The UPS measurements showed that the valence band maximum energy levels (E_{VB}) of TpBpy–Cu and TpBpy–Cu/Co were −5.05 and −5.04 eV, respectively (Fig. 4c). The E_{VB} of TpBpy was −5.58 eV, as reported in a previous study.[32] Based on the equation $E_{CB} = E_{BG} + E_{VB}$, the conduction band minimum energy levels (E_{CB}) of the COFs was found to lie above the proton reduction potential (−4.44 eV).[35]

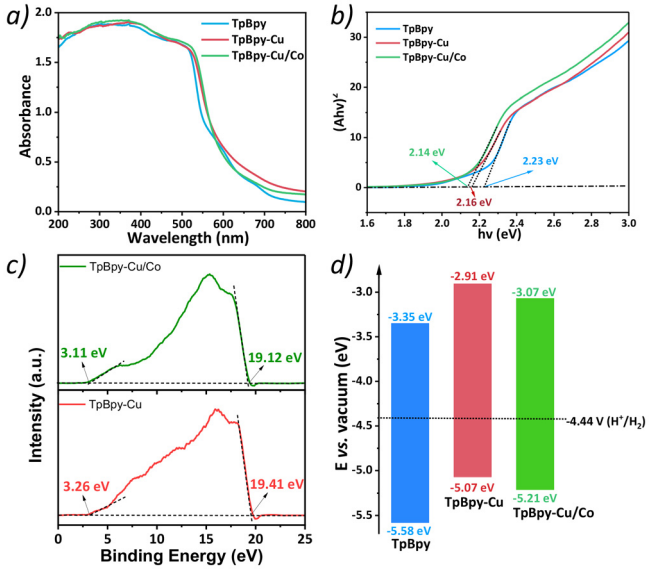

Fig. 4 (a) UV/Vis-DRS spectra of TpBpy, TpBpy–Cu and TpBpy–Cu/Co. (b) Tauc plot of TpBpy, TpBpy–Cu, and TpBpy–Cu/Co. (c) UPS spectra of TpBpy–Cu and TpBpy–Cu/Co. (d) Energy band diagrams of TpBpy, TpBpy–Cu and TpBpy–Cu/Co.

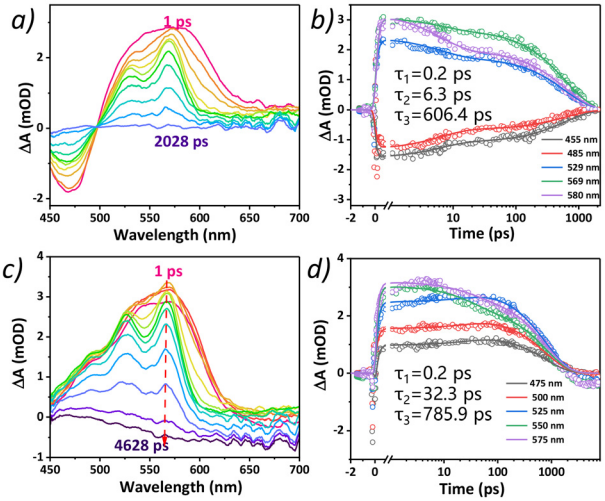

Fig. 5 (a) Ultrafast transient spectra and (b) kinetic fitting of [Cu(mestphen)(bpy)]$^+$ in acetonitrile following 415 nm excitation. (c) Ultrafast transient spectra and (d) kinetic fitting of TpBpy–Cu in acetonitrile following 415 nm excitation.

Obviously, the band structure of TpBpy, TpBpy–Cu, and TpBpy–Cu/Co is thermodynamically sufficient for the photocatalytic hydrogen evolution reaction (HER) (Fig. 4d).

Ultrafast transient optical spectroscopy

To elucidate the influence of confinement on the excited-state kinetics of Cu(I) photosensitizers (PS), we employed ultrafast transient optical spectroscopy to examine the excited-state dynamics of TpBpy–Cu alongside the corresponding Cu(I) diimine complexes, [Cu(mestphen)(bpy)]$^+$. This approach allowed for a detailed investigation into the impact of the confined environment on charge dynamics and energy transfer mechanisms. Utilizing established analysis methods for Cu(I) diimine complexes, the transient absorption data were globally fitted across a broad wavelength range with multi-exponential functions.[36,37] The transient spectra of both [Cu(mestphen)(bpy)]$^+$ and TpBpy–Cu, as shown in Fig. 5, display an initial broad, featureless excited-state absorbance centered around 550 nm. This spectral feature undergoes evolution into a more defined profile characterized by two local absorption maxima at 526 nm and 567 nm. This transformation reflects the intricate interactions occurring within the excited state, which are influenced by the structural characteristics of the COF. The rigid framework of the COF effectively constrains the complexes, limiting their ability to undergo flattening distortions and reducing exposure to the solvent environment following photoexcitation, thus enhancing excited-state lifetimes, resulting in TpBpy–Cu exhibiting a significantly extended lifetime of 785.9 ps compared to the shorter excited-state lifetime of 606.4 ps observed for [Cu(mestphen)(bpy)]$^+$.

The increase in the excited-state lifetime for TpBpy–Cu is particularly beneficial for proton reduction reactions, as it enhances the likelihood of energy transfer processes occurring before non-radiative decay pathways become dominant. This extension of the excited-state lifetime not only facilitates more efficient charge separation but also can improve the overall efficiency of the photocatalytic process. These findings highlight the critical role of the confinement effect in modulating the excited-state behavior of Cu(I) complexes. By effectively restricting structural distortions and minimizing solvent interactions, the COF environment optimizes the performance of the Cu(I) photosensitizer, thereby providing a valuable strategy for enhancing the efficiency of solar-driven energy conversion processes.

Photocatalytic hydrogen production

Photocatalytic hydrogen evolution experiments were conducted under visible light irradiation ($\lambda > 420$ nm), utilizing BIH as a sacrificial electron donor and acetic acid as the proton source.[38] Initially, three TpBpy–Cu/Co samples with varying contents of Cu/Co were tested, among which TpBpy–Cu/Co (Cu/Co = 1.8 : 1) shows the highest photocatalytic H_2 generation rate, as shown in Fig. S9.† Afterwards, water was used to replace acetic acid and the photocatalytic hydrogen production rate decreased from 50.88 to 11.76 mmol g^{-1}, as shown in Fig. S10,† hence DMF/AcOH was used as the reaction medium in subsequent studies. In addition, we compared the photocatalytic hydrogen evolution performances of TpBpy, TpBpy–Cu and TpBpy–Cu/Co without adding the corresponding homogeneous metal complexes, *i.e.* [Cu(mestphen)(bpy)]$^+$ or Co(bpy)Cl_2. The amount of hydrogen produced by pristine TpBpy after 6 h of illumination was 1.60 mmol g^{-1}. With the immobilization of Cu(I), the hydrogen production increased significantly to 13.44 mmol g^{-1}. The photocatalytic perform-

ance of TpBpy–Cu/Co gave the highest H_2 evolution amount of up to 50.88 mmol g^{-1}, approximately 32 times higher than that of TpBpy (Fig. 6a). Notably, TpBpy–Cu/Co demonstrated the highest HER rate of up to 12.16 mmol g^{-1} h^{-1}, 3.6 times higher than TpBpy–Cu and approximately 25 times that of TpBpy (Fig. 6b). To verify the important role of metal coordination, we also compared the photocatalytic HER performance of TpBpy + homogeneous $[Cu(mestphen)(bpy)]^+$ + $Co(bpy)Cl_2$, TpBpy–Cu + homogeneous $Co(bpy)Cl_2$, and TpBpy–Cu/Co, while keeping the content of copper and cobalt the same. TpBpy–Cu + homogeneous $Co(bpy)Cl_2$ and TpBpy + homogeneous $[Cu(mestphen)(bpy)]^+$ + $Co(bpy)Cl_2$ exhibited a lower HER rate of 7.40 and 3.44 mmol g^{-1} h^{-1}, respectively. After 6 h of irradiation, the total hydrogen production was shown to be 50.88 mmol g^{-1} for TpBpy–Cu/Co, 32.08 mmol g^{-1} for TpBpy–Cu + homogeneous $Co(bpy)Cl_2$, and 11.64 mmol g^{-1} for TpBpy + homogeneous $[Cu(mestphen)(bpy)]^+$ + $Co(bpy)Cl_2$ (Table S2†). Moreover, a similar trend was also observed when the catalyst concentration was reduced to one-tenth of its original value (Fig. S11 and Table S3†). We assumed that the superior H_2 production by TpBpy–Cu/Co originated from: (1) improved photosensitizing ability and (2) the proximity of Co and Cu sites, which suppresses electron and hole recombination and promotes the migration of photo-generated charge carriers in COF. Notably, the hydrogen production performance of TpBpy–Cu/Co in this study surpasses that of most non-noble metal photocatalytic systems and progressively narrows the performance gap with noble metal systems (Fig. 6c and Table S4†).

To examine the transfer kinetics of the photogenerated carriers, photo/electrochemical measurements were conducted. The dynamics of charge carriers in the COFs were investigated using measurements of electrochemical impedance spectroscopy (EIS) and transient photocurrents. Among them, TpBpy–Cu/Co has the highest transient photocurrent and the lowest electron transfer resistance (Fig. 7a and b). This is assumed due to the proximity of the Co(II) and Cu(I) sites, which facilitates more efficient electron transfer in the covalent organic framework, allowing for more effective separation of photogenerated charge carriers.[31]

In order to verify this hypothesis, we carried out steady-state and time-resolved photoluminescence measurements. As shown in Fig. 7c, the photoluminescence (PL) emission was centered at 420 nm, consistent with the results of a previous report.[39] TpBpy–Cu shows significant quenching of fluorescence intensity due to rapid charge transfer between Cu(I) and TpBpy. Furthermore, the much lower fluorescence intensity of TpBpy–Cu/Co suggests that the charge carrier recombination is strongly suppressed, indicating possible electron transfer from TpBpy–Cu to the Co(II) catalytic center. Furthermore, time-resolved PL analysis, shown in Fig. 7d, revealed that the average PL lifetime of TpBpy–Cu/Co (2.83 ns) was twice that of TpBpy (1.65 ns) and TpBpy–Cu (1.35 ns). This enhancement in the excited-state lifetime suggests that the incorporation of Co ions effectively prolongs the persistence of photoinduced charge carriers. As illustrated by the Perrin–Jablonski diagram (Fig. S12†), the shorter lifetime (τ_1) of the excited-state relaxation is generally correlated to the nonradiative relaxation of charge-carriers ($S_n \rightarrow S_1$), and the longer lifetime (τ_2) reflects the radiative recombination of charge-carriers ($S_1 \rightarrow S_0$).[40] The fitted decay lifetimes (τ_1 and τ_2) for TpBpy are 0.96 and 16.51 ns, which account for 95.58% and 4.42% of the total decay, respectively. TpBpy–Cu shows values of 0.84 and 2.73 ns, respectively, corresponding to 72.98% and 27.02%. In the case of TpBpy–Cu/Co, the fitted decay lifetimes (τ_1 and τ_2) are 0.74 and 4.46 ns, respectively,

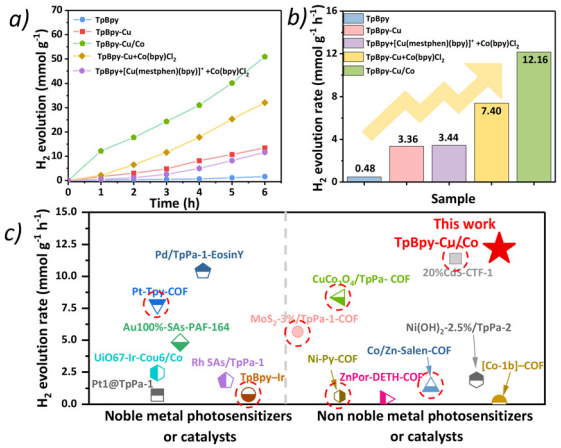

Fig. 6 (a) Time dependent H_2 production under visible light irradiation and (b) photocatalytic H_2 evolution rates of TpBpy, TpBpy–Cu and TpBpy–Cu/Co (0.25 mg COF and 90 mg BIH, in 45 μL AcOH and 2.955 mL DMF). A 300 W xenon lamp with a 420 nm cut off filter (light intensity: 520 mW cm^{-2}) was used as the light source. (c) Comparison of previously reported MOF/COF systems using noble/non-noble metal photosensitizers or catalysts for photocatalytic hydrogen evolution reactions. Note: the red dash circle indicates that the photocatalytic reactions were performed under acidic conditions.

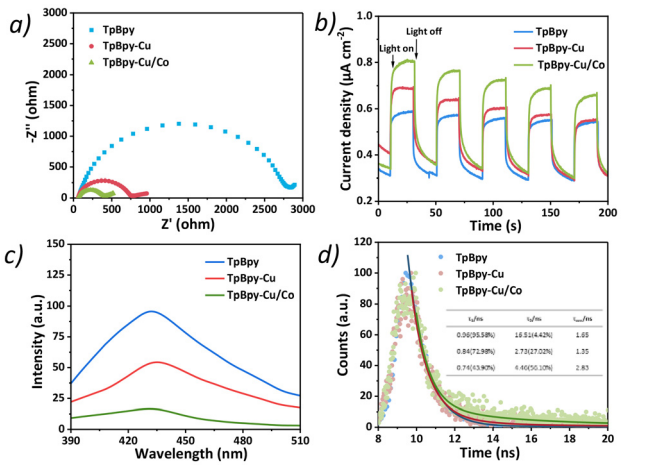

Fig. 7 (a) EIS Nyquist plots and (b) transient photocurrent response of TpBpy, TpBpy–Cu and TpBpy–Cu/Co. (c) Photoluminescence emission spectra and (d) time-resolved photoluminescence spectra at 420 nm (λ_{ex} = 375 nm) of TpBpy, TpBpy–Cu and TpBpy–Cu/Co.

corresponding to 43.90% and 56.10% of the total decay. Based on these results, it is confirmed that TpBpy–Cu/Co and TpBpy–Cu are more efficient at charge separation since the non-radiative deactivation proportion gradually decreases over time.

To gain further insight into the photocatalytic mechanisms, cyclic voltammograms (CVs) of Cu–PS and various catalysts were analyzed, as shown in Fig. S13.† CV scans were first conducted for TpBpy–Cu/Co and $Co(bpy)Cl_2$ under catalytic hydrogen evolution reaction (HER) conditions. The TpBpy–Cu/Co catalyst showed an irreversible catalytic HER peak starting at −0.89 V *vs.* NHE. This indicates that hydrogen production begins after the injection of two electrons, as shown in Fig. 8a. On the other hand, $Co(bpy)Cl_2$ exhibited only an irreversible catalytic HER peak, with an onset potential at −0.96 V *vs.* NHE. The difference in the catalytic behavior of TpBpy–Cu/Co and $Co(bpy)Cl_2$ can be explained by the isolated Co active sites in TpBpy COF and the formation of metallic Co nanoparticles in homogeneous $Co(bpy)Cl_2$ under catalytic HER conditions. A reversible reduction peak at −1.47 V *vs.* NHE was observed for $[Cu(mestphen)(bpy)]^+$, which is assigned to the reduction of the Cu–PS center. Similarly, a reduction peak at −1.32 V was also observed in TpBpy–Cu/Co. The above results illustrate that the reduction of the Cu–PS center can provide adequate driving force for the HER with the Co catalyst (−0.89 V *vs.* NHE).

Based on a previous study[38] and the preceding analysis, we propose the following photocatalytic mechanism for the hydrogen evolution reaction (HER) using TpBpy–Cu/Co, as shown in Fig. 8. Upon irradiation (step 1), the copper photosensitizer (Cu-PS) unit transitions to the excited state [Cu-PS]* (step 2). The excited-state [Cu-PS]* is subsequently reduced by BIH to form $[Cu]^-$ (step 3), which then transfers electrons into the cobalt sites, thereby promoting the HER and returning to the ground state (step 4). Concurrently, cobalt is reduced from Co (II) to Co(0) (step 4). The active Co(0) species then participates in proton reduction to produce H_2, while regenerating the initial complex structure (step 5).

Control photocatalytic experiments were conducted on TpBpy–Cu/Co to determine the importance of each component (acetic acid, BIH, and light) in the photocatalytic hydrogen evolution reaction (Fig. S14†). The production of hydrogen was almost non-existent in the absence of acetic acid, BIH, or light. According to these results, proton sources, sacrificial electron donors, and light sources are all crucial components of photocatalytic HER. A light-on/light-off experiment was conducted, which also indicates that the hydrogen evolution reaction of TpBpy–Cu/Co is driven by visible light irradiation (Fig. S15†).

To assess the stability and reusability of TpBpy–Cu/Co, we conducted a series of recycling tests focused on the photocatalytic hydrogen evolution reaction (HER). Over three consecutive cycles, TpBpy–Cu/Co exhibited minimal loss of activity, as shown in Fig. 9a. The initial decline in the hydrogen evolution rate observed during the first 3–6 h (Fig. 9a) is attributable to the absence of BIH. The subsequent addition of BIH at the start of the second cycle effectively restored the hydrogen evolution rate to its baseline value. However, the photocatalytic performance of TpBpy–Cu/Co could not be fully restored after extended irradiation, as indicated by a decrease in the H_2 production rate commencing after the third cycle. Nevertheless, the transient photocurrent unchanged and charge transfer resistance of TpBpy–Cu/Co increased following photocatalysis compared to its initial state (Fig. 9b and Fig. S16†). The FT-IR and PXRD results confirmed that the crystallinity and chemical composition of TpBpy–Cu/Co remained unchanged after 24 hours of photocatalysis (Fig. 9c and d). XPS analysis, shown in Fig. S17,† revealed peaks at

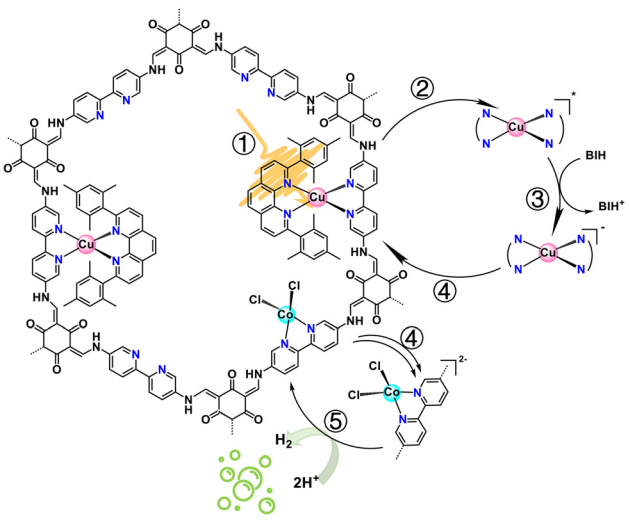

Fig. 8 Proposed photocatalytic mechanism of TpBpy–Cu/Co for the HER.

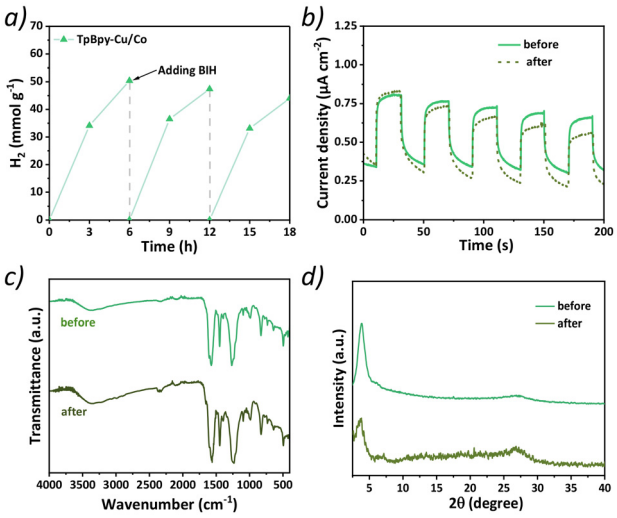

Fig. 9 (a) Cycling test of photocatalytic H_2 evolution under visible light irradiation. (b) Transient photocurrent response. (c) FT-IR spectra. (d) XRD patterns of TpBpy–Cu/Co before and after 24 h photocatalysis.

952.1 eV and 932.3 eV, corresponding to Cu(I) $2p_{1/2}$ and Cu(I) $2p_{3/2}$, respectively, and small peaks at 954.7 eV and 934.7 eV, corresponding to Cu(II) $2p_{1/2}$ and Cu(II) $2p_{3/2}$. The Co(II) 2p XPS spectrum for TpBpy–Cu/Co displays characteristic peaks at 781.1 eV (Co(II) $2p_{3/2}$) and 797.0 eV (Co(II) $2p_{1/2}$). The comparison of XPS analysis before and after photocatalysis further confirm the stability of TpBpy–Cu/Co.

Experimental section

Materials

All ligands, salts, other reagents, and solvents were purchased from commercial sources and used as received. TpBpy was synthesized according to previously reported procedures.[41]

Physical methods

Nuclear magnetic resonance (NMR) spectra were recorded on a Bruker Avance III HD 400 MHz. ^{1}H NMR spectra were referenced to TMS using the residual solvent peak. All chemical shifts are reported in standard δ notation (in parts per million); positive chemical shifts are at a higher frequency than the reference. High resolution mass spectra (HRMS) were acquired using a Bruker ESI-Q-TOF MS/MS. Powder X-ray diffraction (PXRD) patterns were recorded on a Bruker D8 Discover with Cu-Kα radiation. N_2 adsorption–desorption isotherms were collected using a Micromeritics ASAP 2460 at 77 K, and the surface area and pore size distribution were calculated by BET and NL-DFT methods. UV-vis spectroscopy in solution and solid state and FTIR were carried out using an Agilent Cary 60, Shimadzu UV-2600i, and PerkinElmer Spectrum 100, respectively. Thermogravimetric analysis (TGA) was conducted on a Shimadzu DTG-60A thermal analyzer under N_2 with the temperature ramped from 25 °C to 800 °C at the rate of 10 °C min^{-1}. X-ray photoelectron spectroscopy (XPS) was performed on an AXIS SUPRA with an Al-Kα radiation source. The metal content was measured by inductively coupled plasma-mass spectrometry (ICP-MS) using an Agilent 7800. Scanning electron microscopy (SEM) images were observed using a JSM-IT500HR device. Transmission electron microscopy (TEM) images were observed using a Talos F200X G2. Amounts of H_2 generated in the photocatalytic experiments were determined by gas chromatography (GC) using a Techcomp GC7980 with argon as the carrier gas and a TCD or an FID detector. The lifetimes of the fluorescence spectra were examined using an FLS1000 (Edinburgh Instruments, UK) equipped with a 375 nm laser as the excitation source and employing the Time Correlated Single Photon Counting (TCSPC) technique. Electrochemical properties were measured on a CH Instruments CHI-760E bi-potentiostat at ambient temperature (21–24 °C). The electrochemical performance was conducted using a three-electrode system with a glassy carbon as the working electrode, Ag/AgCl (3M) as the reference electrode and platinum as the counter electrode. UV photoelectron spectra of the COFs were obtained using a monochromatic He I (21.22 eV) light source, with an energy resolution of 100 meV.

Synthesis of materials

[Cu(mestphen)(bpy)]$^+$. Following the "HETPHEN" method for the synthesis of heteroleptic copper(I)bis(phen) complexes, tetrakis(acetonitrile)copper(I) hexafluorophosphate (37 mg, 0.1 mmol, 1 eq.) was dissolved in 10 mL dichloromethane and purged with nitrogen for 10 minutes. 2,9-dimesitylphenanthroline (42 mg, 0.1 mmol, 1 eq.) in 10 mL degassed CH_2Cl_2 was added under a nitrogen atmosphere and stirred for five minutes. Bipyridine (15.6 mg, 0.1 mmol, 1 eq.) was then added, and the reaction mixture was stirred at ambient temperature under nitrogen for 1 hour. The red solution was filtered to remove any insoluble material. The solvent was removed by rotary evaporation and the red solid was re-dissolved in a minimal amount of dichloromethane and layered with diethyl ether. The product was collected by filtration using a fritted funnel (yield 85%). ^{1}H NMR (500 MHz, DMSO-d_6) δ 8.93 (d, J = 8.1 Hz, 2H), 8.37 (s, 2H), 8.21 (dd, J = 36.5, 6.6 Hz, 4H), 8.01 (dd, J = 11.8, 7.5 Hz, 4H), 7.46 (t, J = 6.3 Hz, 2H), 6.19 (s, 4H), 1.86 (s, 6H), 1.71 (s, 12H). ^{13}C NMR (500 MHz, DMSO-d_6) δ 158.08, 150.69, 148.22, 143.14, 137.50, 137.25, 137.11, 136.84, 134.25, 127.48, 126.96, 126.60, 126.47, 125.46, 120.91, 20.29, 19.68.

Co(bpy)Cl$_2$. Co(bpy)Cl_2 was prepared according to a documented procedure:[3] Bipyridine (2 mmol) and anhydride cobalt chloride (2 mmol) were added to THF (5 mL) in a 50 mL round bottom flask under an argon atmosphere. The reaction mixture was stirred for 10 h at room temperature and diethyl ether was added to fully precipitate the dusty blue solid. The solvent was decanted out of the flask using a pipette, the solid was washed thoroughly with ether three times and dried under vacuum to yield the Co(bpy)Cl_2 complex (544 mg, 95% yield). HRMS (ESI-MS) calcd for $C_{10}H_8ClCoN_2$ [M-Cl]$^+$: 249.9703, found: 249.9719.

TpBpy. A Pyrex tube (10 mL) was charged with Tp (21.0 mg, 0.1 mmol), Bpy (27.9 mg, 0.15 mmol), mesitylene (0.5 mL), dioxane (0.5 mL) and 6 M HAc (0.1 mL). The mixture was sonicated for 10 min and then degassed *via* three freeze–pump–thaw cycles before sealing under vacuum. The sealed tube was kept at 120 °C in an oven for 3 days and cooled to room temperature. The precipitate was collected by filtration and washed with THF and acetone several times. Then the product was Soxhlet-extracted with THF for 1 day and dried under vacuum at 40 °C for 24 h to obtain TpBpy-COF powder (40 mg, 92%).

TpBpy–Cu. In a glovebox, Cu$(CH_3CN)_4PF_6$ (26.1 mg, 0.07 mmol) and 2,9-dimesitylphenanthroline (29.4 mg, 0.07 mmol) were dissolved in 5 mL of CH_2Cl_2 and stirred for 5 minutes. 40 mg TpBpy was added to the vial and the mixture was stirred inside the glovebox for 48 h. The resultant red solid was separated by centrifugation and washed with CH_2Cl_2 several times to remove excess Cu salt. Cu loading was determined by ICP-MS and could be controlled by adjusting the equivalents of the Cu salt added and the reaction time.

TpBpy–Cu/Co. In a glovebox, the red solid TpBpy–Cu, obtained above, was further stirred with $CoCl_2$ (0.015 mmol, 1.95 mg) in 5 mL MeOH at room temperature for 18 h and

then thoroughly washed with MeOH to afford TpBpy–Cu/Co in a near-quantitative yield. ICP-MS analysis of TpBpy–Cu/Co revealed a Cu : Co ratio of 1.8 : 1.

Electrochemical measurements

Electrochemical measurements were performed with a CH Instruments CH-760E bipotentiostat at ambient temperature (21–24 °C) in a single compartment cell with a 3.0 mm glassy carbon disc as the working electrode, a platinum wire as the counter electrode, and Ag/AgCl (3 M NaCl) as the reference electrode. The catalyst (5 mg) was dispersed into a solution of 50 μL 5 wt% Nafion and 1 mL ethanol. The suspension was drop-cast sequentially (5 μL × 2) on the surface of the electrode, allowing each drop to dry completely before applying the next. Electrochemical impedance spectroscopy (EIS) and photocurrent measurements were carried out in 0.2 M Na_2SO_4 solution as the supporting electrolyte.

Visible light-driven hydrogen evolution reaction (HER)

Photocatalytic HERs were carried out in an externally illuminated reaction vessel with a magnetic stirrer. Samples were prepared in 5.5 mL septum-sealed quartz vials. In a standard reaction (Table S2, entry 1†), each sample was made up to a volume of 3.000 mL including 2.955 mL DMF, 0.045 mL AcOH, and 90 mg BIH (0.40 mmol) in addition to a specified amount of the COF catalyst. Sample vials were capped and sealed and deoxygenated by bubbling nitrogen for 10 min to ensure complete air removal. The solution was irradiated using a 300 W xenon lamp with a 420 nm cut off filter (light intensity: 520 mW cm^{-2}). The reaction temperature was kept below 30 °C during the irradiation. After the hydrogen evolution reaction, the gas in the headspace of the vial was analyzed by GC to determine the amount of hydrogen generated. The hydrogen evolution rate is calculated by dividing the molar amount of H_2 produced by the product of catalyst mass and hours of irradiation.

Light on–off experiment catalyzed photocatalytic HER

Light on–off experiments with a short period of light irradiation were conducted to confirm the photocatalytic nature of the TpBpy–Cu/Co or TpBpy–Cu catalyzed HER and to determine the hydrogen evolution rate. Under standard photocatalytic HER conditions, the hydrogen generation of both TpBpy–Cu/Co and TpBpy–Cu was monitored after 1 h of light irradiation followed by 1 h in the dark. This cycle was repeated for 4 times. H_2 production gradually increased under light irradiation but stopped in the dark. The HER was thus confirmed to be driven by visible light. The time-dependent hydrogen evolution rate curves of both TpBpy–Cu/Co and TpBpy–Cu were calculated based on average H_2 production rate (h^{-1}) during each light irradiation period.

Recycle tests of TpBpy–Cu/Co catalyzed photocatalytic HER

Recycle tests of TpBpy–Cu/Co for photocatalytic HER were carried out to demonstrate the stability and reusability of the present COF system. Under photocatalytic HER conditions, TpBpy–Cu/Co was recycled and reused without significant loss of activity for at least 3 consecutive runs. Specifically, HER recycle reactions were conducted with TpBpy–Cu/Co (0.136 μmol Cu site, 0.075 μmol Co site) and 90 mg BIH in a solvent mixture of 45 μL AcOH + 2.955 mL DMF, under the irradiation of a 300 W xenon lamp with a 420 nm cut off filter (light intensity: 520 mW cm^{-2}). The solution was degassed with N_2 for 10 min before each run and 10 mg of BIH was added to the solution after each run.

Conclusions

In summary, we have developed a novel heterogeneous photocatalytic system for HER *via* dual metalation of TpBpy COF. The successful functionalization of the COF with Cu(I) and Co(II) metal units was confirmed by BET, ICP, EDS, and XPS. The Cu(I) unit in the COF increased the photosensitizing capability and the Co(II) unit enhanced the catalytic H_2 production. In this study, TpBpy not only serves as an effective platform for the heterogenization of metal complexes but also plays a crucial role in spatially confining the Cu(I) photosensitizer, thereby enhancing its photophysical properties. Moreover, dual metalation of both Cu(I) and Co(II) improves charge separation and transfer, ultimately enhancing photocatalysis. This unique arrangement improves the overall efficiency of the photocatalytic process while maintaining the stability of the metal sites. Overall, this work presents a novel and promising heterogeneous platform for photocatalytic hydrogen evolution, combining the benefits of both homogeneous and heterogeneous catalysis, including improved sustainability, ease of separation, and enhanced recyclability. By integrating non-noble metals with well-defined COFs, we pave the way for more efficient, durable, and scalable photocatalytic systems in the pursuit of sustainable energy solutions.

Author contributions

Conceptualization: L. W.; investigation: M. S. and A. W.; formal analysis: M. S., J. P, and L. W; writing original draft: M. S.; and writing, review and editing: X. S. and L. W.

Data availability

The data supporting this article have been included as part of the ESI.†

Conflicts of interest

There are no conflicts to declare.

Acknowledgements

This work was supported by the National Natural Science Foundation of China (22205144). This work was carried out at the University of Shanghai for Science and Technology. The authors would like to thank the Center for Instrumental Analysis, the University of Shanghai for Science and Technology and the Shiyanjia Lab (**https://www.shiyanjia.com**).

References

1 X. Sun, S. Jiang, H. Huang, H. Li, B. Jia and T. Ma, Solar energy catalysis, *Angew. Chem.*, 2022, **134**, e202204880.
2 Q. Zhu, Q. Xu, M. Du, X. Zeng, G. Zhong, B. Qiu and J. Zhang, Recent progress of metal sulfide photocatalysts for solar energy conversion, *Adv. Mater.*, 2022, **34**, 2202929.
3 S. E. Hosseini and M. A. Wahid, Hydrogen from solar energy, a clean energy carrier from a sustainable source of energy, *Int. J. Energy Res.*, 2020, **44**, 4110–4131.
4 Q. Hassan, A. M. Abdulateef, S. A. Hafedh, A. Al-samari, J. Abdulateef, A. Z. Sameen, H. M. Salman, A. K. Al-Jiboory, S. Wieteska and M. Jaszczur, Renewable energy-to-green hydrogen: A review of main resources routes, processes and evaluation, *Int. J. Hydrogen Energy*, 2023, **48**, 17383–17408.
5 M. Ismael, A review and recent advances in solar-to-hydrogen energy conversion based on photocatalytic water splitting over doped-TiO_2 nanoparticles, *Sol. Energy*, 2020, **211**, 522–546.
6 Y. Wang, Y. Zhao and Z. Li, 2D covalent organic frameworks as photocatalysts for solar energy utilization, *Macromol. Rapid Commun.*, 2022, **43**, 2200108.
7 T. He and Y. Zhao, Covalent organic frameworks for energy conversion in photocatalysis, *Angew. Chem., Int. Ed.*, 2023, **62**, e202303086.
8 D.-G. Wang, T. Qiu, W. Guo, Z. Liang, H. Tabassum, D. Xia and R. Zou, Covalent organic framework-based materials for energy applications, *Energy Environ. Sci.*, 2021, **14**, 688–728.
9 R. Chen, Y. Wang, Y. Ma, A. Mal, X.-Y. Gao, L. Gao, L. Qiao, X.-B. Li, L.-Z. Wu and C. Wang, Rational design of isostructural 2D porphyrin-based covalent organic frameworks for tunable photocatalytic hydrogen evolution, *Nat. Commun.*, 2021, **12**, 1354.
10 S. Liu, M. Wang, Y. He, Q. Cheng, T. Qian and C. Yan, Covalent organic frameworks towards photocatalytic applications: Design principles, achievements, and opportunities, *Coord. Chem. Rev.*, 2023, **475**, 214882.
11 H. Yang, M. Hao, Y. Xie, X. Liu, Y. Liu, Z. Chen, X. Wang, G. I. Waterhouse and S. Ma, Tuning local charge distribution in multicomponent covalent organic frameworks for dramatically enhanced photocatalytic uranium extraction, *Angew. Chem., Int. Ed.*, 2023, **62**, e202303129.
12 I. E. Khalil, P. Das and A. Thomas, Two-Dimensional Covalent Organic Frameworks: Structural Insights across Different Length Scales and Their Impact on Photocatalytic Efficiency, *Acc. Chem. Res.*, 2024, 4712–19803.
13 J. Huang, X. Liu, W. Zhang, Z. Liu, H. Zhong, B. Shao, Q. Liang, Y. Liu and Q. He, Functionalization of covalent organic frameworks by metal modification: Construction, properties and applications, *Chem. Eng. J.*, 2021, **404**, 127136.
14 J. Dong, X. Han, Y. Liu, H. Li and Y. Cui, Metal–covalent organic frameworks (MCOFs): a bridge between metal–organic frameworks and covalent organic frameworks, *Angew. Chem., Int. Ed.*, 2020, **59**, 13722–13733.
15 D. A. Popov, J. M. Luna, N. M. Orchanian, R. Haiges, C. A. Downes and S. C. Marinescu, A 2, 2′-bipyridine-containing covalent organic framework bearing rhenium(I) tricarbonyl moieties for CO_2 reduction, *Dalton Trans.*, 2018, **47**, 17450–17460.
16 Y. Yin and G. Liu, A covalent organic framework containing bipyridine groups as a fluorescent chemical probe for the ultrasensitive detection of arsenic(III), *J. Photochem. Photobiol., A*, 2021, **421**, 113528.
17 T. Kim, D.-Y. Lee, E. Choi, H.-i. Kim and B.-S. Kim, Simultaneous Photocatalytic Hydrogen Peroxide Production and Pollutant Degradation via Bipyridine-Based Polyimide Covalent Organic Framework, *Appl. Catal., B*, 2024, 124264.
18 X. Li, Q. Yang, Y. Yuan, Y. Shama and H. Yan, Inhibiting Photo–Oxidation and Enhancing Visible–Light–Driven Photocatalytic Water Oxidation over Covalent Organic Frameworks Through the Coordination of Cobalt with Bipyridine, *Small*, 2024, 2401168.
19 W. Zhong, R. Sa, L. Li, Y. He, L. Li, J. Bi, Z. Zhuang, Y. Yu and Z. Zou, A covalent organic framework bearing single Ni sites as a synergistic photocatalyst for selective photoreduction of CO_2 to CO, *J. Am. Chem. Soc.*, 2019, **141**, 7615–7621.
20 F. Muniz-Miranda, L. De Bruecker, A. De Vos, F. Vanden Bussche, C. V. Stevens, P. Van Der Voort, K. Lejaeghere and V. Van Speybroeck, Optical properties of isolated and covalent organic framework-embedded ruthenium complexes, *J. Phys. Chem. A*, 2019, **123**, 6854–6867.
21 D. Song, W. Xu, W. He, C. Li, J. Yang, J. Li and N. Wang, Selective Integrating Molecular Catalytic Units into Bipyridine-Based Covalent Organic Frameworks for Specific Photocatalytic Fuel Production, *Inorg. Chem.*, 2024, **63**, 3444–3451.
22 Y. Zhang, M. Schulz, M. Wächtler, M. Karnahl and B. Dietzek, Heteroleptic diimine–diphosphine Cu(I) complexes as an alternative towards noble-metal based photosensitizers: Design strategies, photophysical properties and perspective applications, *Coord. Chem. Rev.*, 2018, **356**, 127–146.
23 M. V. Appleby, P. G. Walker, D. Pritchard, S. van Meurs, C. M. Booth, C. Robertson, M. D. Ward, D. J. Kelly and J. A. Weinstein, Cu(I) diimine complexes as immobilised antibacterial photosensitisers operating in water under visible light, *Mater. Adv.*, 2020, **1**, 3417–3427.
24 Y. Yamazaki, T. Onoda, J. Ishikawa, S. Furukawa, C. Tanaka, T. Utsugi and T. Tsubomura, Photocatalytic CO_2 reduction using various heteroleptic diimine-diphosphine

Cu(I) complexes as photosensitizers, *Front. Chem.*, 2019, **7**, 288.

25 M. Iwamura, S. Takeuchi and T. Tahara, Ultrafast excited-state dynamics of copper(I) complexes, *Acc. Chem. Res.*, 2015, **48**, 782–791.

26 N. A. Gothard, M. W. Mara, J. Huang, J. M. Szarko, B. Rolczynski, J. V. Lockard and L. X. Chen, Strong steric hindrance effect on excited state structural dynamics of Cu (I) diimine complexes, *J. Phys. Chem. A*, 2012, **116**, 1984–1992.

27 S.-P. Luo, L.-Z. Tang and S.-Z. Zhan, A cobalt(II) complex of 2, 2-bipyridine, a catalyst for electro-and photo-catalytic hydrogen production in purely aqueous media, *Inorg. Chem. Commun.*, 2017, **86**, 276–280.

28 J. Dong, M. Wang, P. Zhang, S. Yang, J. Liu, X. Li and L. Sun, Promoting effect of electrostatic interaction between a cobalt catalyst and a xanthene dye on visible-light-driven electron transfer and hydrogen production, *J. Phys. Chem. C*, 2011, **115**, 15089–15096.

29 Z. Chen, M. Yang, Z. Li, W. Liao, B. Chen, T. Yang, R. Hu, Y. Yang and S. Meng, Highly sensitive and convenient aptasensor based on Au NPs@ Ce-TpBpy COF for quantitative determination of zearalenone, *RSC Adv.*, 2022, **12**, 17312–17320.

30 R. Bu, L. Zhang, L.-L. Gao, W.-J. Sun, S.-L. Yang and E.-Q. Gao, Copper(I)-modified covalent organic framework for CO_2 insertion to terminal alkynes, *Mol. Catal.*, 2021, **499**, 111319.

31 A. Jati, K. Dey, M. Nurhuda, M. A. Addicoat, R. Banerjee and B. Maji, Dual Metalation in a Two-Dimensional Covalent Organic Framework for Photocatalytic C–N Cross-Coupling Reactions, *J. Am. Chem. Soc.*, 2022, **144**, 7822–7833.

32 M. Zhou, Z. Wang, A. Mei, K. Chen, J. Zeng, Y. Liu and W. Chen, Chemically bonded interface construction of the covalent organic framework/$CsPbBr_3$ heterojunction for efficient photocatalytic CO_2 reduction driven by visible light, *J. Mater. Chem. A*, 2024, **12**, 28283–28295.

33 W. Weng, Z. Lin, H. Zhang, F. Niu, C. Wang, K. Hu and J. Guo, Effect of ESIPT-Induced Photoisomerization of Keto–Enamine Linkages on the Photocatalytic Hydrogen Evolution Performance of Covalent Organic Frameworks, *JACS Au*, 2023, **3**, 3391–3399.

34 B. Tan, B. Xiang, S. Zhang, Y. Qiang, L. Xu, S. Chen and J. He, Papaya leaves extract as a novel eco-friendly corrosion inhibitor for Cu in H_2SO_4 medium, *J. Colloid Interface Sci.*, 2021, **582**, 918–931.

35 G. Fu, D. Yang, S. Xu, S. Li, Y. Zhao, H. Yang, D. Wu, P. S. Petkov, Z.-A. Lan, X. Wang and T. Zhang, Construction of Thiadiazole-Bridged sp^2-Carbon-Conjugated Covalent Organic Frameworks with Diminished Excitation Binding Energy Toward Superior Photocatalysis, *J. Am. Chem. Soc.*, 2024, **146**, 1318–1325.

36 L. Kohler, D. Hayes, J. Hong, T. J. Carter, M. L. Shelby, K. A. Fransted, L. X. Chen and K. L. Mulfort, Synthesis, structure, ultrafast kinetics, and light-induced dynamics of CuHETPHEN chromophores, *Dalton Trans.*, 2016, **45**, 9871–9883.

37 L. Kohler, R. G. Hadt, D. Hayes, L. X. Chen and K. L. Mulfort, Synthesis, structure, and excited state kinetics of heteroleptic Cu(I) complexes with a new sterically demanding phenanthroline ligand, *Dalton Trans.*, 2017, **46**, 13088–13100.

38 X. Feng, Y. Pi, Y. Song, C. Brzezinski, Z. Xu, Z. Li and W. Lin, Metal–Organic Frameworks Significantly Enhance Photocatalytic Hydrogen Evolution and CO_2 Reduction with Earth-Abundant Copper Photosensitizers, *J. Am. Chem. Soc.*, 2020, **142**, 690–695.

39 H. Zhang, Z. Lin, P. Kidkhunthod and J. Guo, Stable immobilization of nickel ions on covalent organic frameworks for panchromatic photocatalytic hydrogen evolution, *Angew. Chem.*, 2023, **135**, e202217527.

40 L. Zhang, C. Wang, Q. Jiang, P. Lyu and Y. Xu, Structurally Locked High-Crystalline Covalent Triazine Frameworks Enable Remarkable Overall Photosynthesis of Hydrogen Peroxide, *J. Am. Chem. Soc.*, 2024, **146**(43), 29943–29954.

41 J. L. Segura, M. J. Mancheño and F. Zamora, Covalent organic frameworks based on Schiff-base chemistry: synthesis, properties and potential applications, *Chem. Soc. Rev.*, 2016, **45**, 5635–5671.